Pergamon

Int. J. Heat Mass Transfer. Vol. 38, No. 3, pp. 419–432, 1995

0017-9310/95 $9.50+0.00

0017-9310(94)00170-7

Heat transfer between a rotating cylinder and a moist granular bed

CHARLES A. COOK and VIC A. CUNDY†

Department of Mechanical Engineering, Louisiana State University, Baton Rouge, LA 70803, U.S.A.

(*Received* 11 *April* 1994 *and in final form* 7 *June* 1994)

Abstract—A model is developed which describes the heat transfer process between the rotating wall of a desorber and an adjacent bed of wet, granular solids. A heat-balance integral method is used. This solution includes the effects of water evaporation near the wall and a thermal contact resistance between the wall and the first layer of particles. The model allows for water evaporation before the bulk bed temperature reaches the saturation temperature of the water. Experimentally measured evaporation rates compare favorably to those predicted by the model. In particular, the water evaporation that occurs before the bulk bed temperature reaches the water saturation temperature is predicted.

INTRODUCTION

Rotating cylinders are commonly used to process solid materials. Examples include rotary kilns and desorbers which are used to heat solid materials. In these applications, the cylinders are usually slightly inclined to horizontal so that the solids move along the axis of rotation. This process is illustrated in Fig. 1, which shows the solids bed which forms near the bottom of the cylinder. Heat is exchanged between the rotating cylinder wall and the solids as the wall passes under the solids bed. Heat is also transferred to the solids from the freeboard gases and the exposed wall surface via convection and radiation. However, in applications involving relatively low temperatures (gas and wall temperatures of approx. 300°C), the wall-to-bed heat transfer becomes the dominant mechanism [1, 2]. These conditions are typical of those found in rotary desorbers used to remediate contaminated soils. In this application, soils are heated to a specified temperature and maintained at this temperature for a time period sufficiently long to desorb contaminants. The temperature history of the soil has been shown to be critical in determining the rate of contaminant desorption and the final level of decontamination [1, 3–9]. Since the soils will usually contain some amount of liquid water, a portion of the heat transferred to the solids is used to evaporate this moisture. The water evaporation rate can significantly affect the temperature history of the solids, thereby affecting the effectiveness of the desorption process. The concentration of water is often much greater than that of contaminants so that the contaminants can be neglected in the heat transfer analysis; the contaminant desorption rate is determined primarily by the temperature-dependent partitioning between the contaminant and the soil particles.

†Author to whom correspondence should be addressed.

Several previous modeling efforts have attempted to predict the effects of moisture content on the axial temperature profile of solids in rotary desorbers and kilns [1, 10–12]. This is accomplished in these models by including a constant-temperature region in the axial temperature profile when the bulk bed temperature reaches the saturation temperature of the moisture. During this constant-temperature period, all heat transferred to the bed is applied toward evaporating moisture. These models, however, do not include the effects of moisture evaporation within the bed on the rate of heat transfer to the solids. Moreover, they assume that no water evaporates before the bulk bed temperature reaches the saturation temperature.

This paper presents and evaluates an analytical model that predicts the rate of heat transfer between a heated rotating cylinder wall and an adjacent granular medium with an initial liquid water content equal to 2–7% of the mass of the dry solids. The model also predicts the rate of water evaporation that results from this heat transfer. In doing so, the effects of the evaporation on the wall-to-bed heat transfer rate are included along with evaporation prior to the bulk bed temperature reaching the saturation temperature. Evaporation rates predicted by the model are compared to those measured experimentally.

BACKGROUND

Heat transfer to the solids bed is dependent, in part, upon the motion of the bed. Several investigators [13–17] have studied the motion of granular beds in rotating cylinders. These studies show that the bed motion can be described in terms of two bed regions, as shown in Fig. 2. The first region, called the static region, consists of particles that have no motion relative to the rotating cylinder. Particles in the static

NOMENCLATURE

a, b	coefficients of the heat-balance integral temperature profiles
A	heat-balance integral parameter defined by equation (27)
c_p	specific heat of solid particle
D	inside diameter of desorber
D_p	characteristic particle dimension
Fo	Fourier number defined by equation (38)
H_v	heat of vaporization of water
h_c	contact heat transfer coefficient
K	permeability
k	thermal conductivity
m''_{evap}	mass flux of water vapor generated at the phase-change interface
$(m'_v)_x$	x-direction mass flow rate of vapor per unit length of desorber
p	pressure
q''	heat flux
s_r	sum of the particle and wall roughnesses
T	temperature
t	time for which a particle at location x has been in contact with the rotating wall
u_v	x-direction Darcy velocity of water vapor
u_s	speed of solids moving with wall
X	mass of moisture in solids bed per mass of dry bed
x	axis along covered wall
y	axis perpendicular to covered wall.

Greek symbols

α_e	effective thermal diffusivity of dry layer including convective effects
α_m	thermal diffusivity of moist solids bed
Δ	dimensionless thickness of dry layer
δ	thickness of dry layer
δ_m	thickness of thermal layer in moist bed region
ε	bed porosity
θ	temperature relative to T_{sat}
ν	kinematic viscosity
ρ	density
ρ_p	density of solid particle
ρ'_L	mass of water per unit mass of dry bed
σ	reduced mean molecular free path
ω	angular rotation rate of wall (rad s^{-1}).

Subscripts

m	moist bed region
s, b	solids bed
sat	saturation conditions
v	water vapor
w	wall
w–b	wall-to-bed.

region move with the rotating wall until they enter the second region, call the shear zone. In the shear zone, particles move down the face of the bed, resulting in the mixing of bed particles. Several studies [15, 18] have suggested that this mixing action produces an approximately isothermal bed.

Several models have utilized the simple bed motion in the static layer and the approximate isothermal nature of the bed to predict heat transfer between a rotating wall and a bed of dry, granular solids. Wes *et al.* [19] propose a simple penetration model in which heat is conducted to the bed particles as they move with the rotating wall. This model assumes that the bulk of the bed is perfectly mixed and that the particles are at the bulk temperature of the bed when they first contact the wall. Lehmberg and Schugerl [15] use a similar penetration approach, but include a thermal contact resistance between the wall and the first layer of bed particles. This thermal contact resistance has been studied by a number of investigators [20–28] and is a function of particle size and shape, particle and surface roughnesses, and interstitial gas properties.

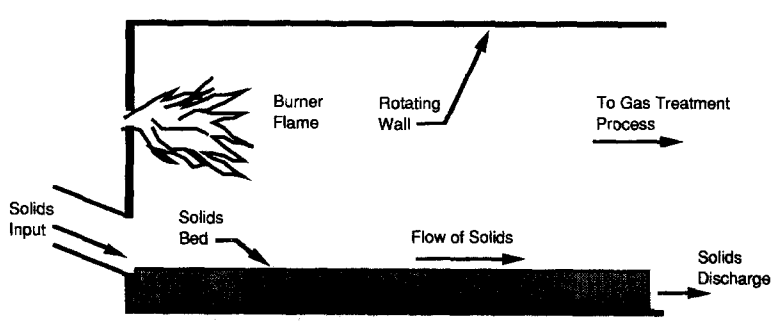

Fig. 1. Schematic diagram of a rotary desorber.

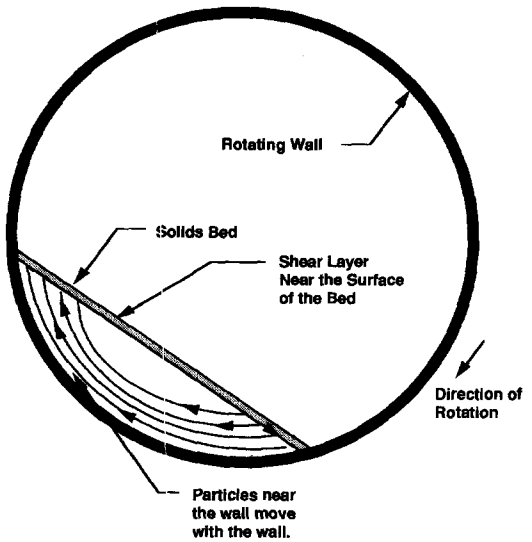

Fig. 2. Bed motion in a rotating cylinder.

Penetration models, with and without thermal contact resistances, have also been used to describe heat transfer between heated surfaces and flowing, agitated, and fluidized beds [23, 25, 28–38]. These models generally assume that the granular bed is dry, semi-infinite, and, except for a region immediately adjacent to the wall, homogeneous. Thus, they do not address the problems encountered with the evaporation of moisture within the bed. When moisture is present in the bed, the particles near the hot wall may be dry while the remainder of the bed is moist. In this situation, the bed is clearly not homogeneous and, due to evaporation within the bed, the problem is no longer one of pure conduction. Schlünder and Mollekopf [39] consider the drying of a mechanically agitated granular bed heated by an adjacent surface. In this model, a uniformly moist bed of particles contacts the heated surface, and the particles adjacent to the surface are heated and dried. An interface dividing these dry particles from the remainder of the moist bed propagates away from the surface. At some time after this process has begun, the bed is assumed to be mechanically agitated, causing the hot, dry particles to become uniformly dispersed with the remainder of the bed. The process is then repeated with an interface moving through the mixture of moist and dry particles. These authors mathematically pose this moving boundary process as a Stefan problem. The Stefan problem, as applied to this process, involves transient conduction from a heated wall (maintained at a constant temperature) through the dry particles near the surface. The temperature at the interface is assumed to be the bulk temperature of the bed. Evaporation occurs only at the interface, and all heat conducted to the interface is applied toward evaporation. From this model, the authors define a surface-to-bed heat transfer resistance which is then placed in series with a thermal contact resistance to obtain an overall surface-to-bed heat transfer resistance. Stefan-type models have also been used to describe the evaporation from an exposed, heated surface of a porous material [40–43].

Evaporation in a static, porous medium adjacent to a vertical or inclined surface has been studied by Rubin and Schweitzer [44], Parmentier [45] and Cheng and Verma [46]. Similar to the Schlünder and Mollekopf [39] agitated bed model, these models consider two regions within the porous medium: a layer immediately adjacent to the heated surface in which the pore volume is completely filled with vapor and a region further from the surface in which the pore volume is liquid-filled. The two regions are separated by a phase-change interface. Essome and Orozco [47] use a similar approach, but extend the analysis to include a binary mixture as the interstitial fluid. Condensation in a porous medium along an inclined surface is considered by Cheng [48]. These phase-change models for porous media differ from the current situation in that the surfaces and solids are stationary, and spatial variations result from the convection of the interstitial fluid phase.

The methods proposed in the literature for calculating heat transfer between surfaces and granular media generally assume that the surface is maintained at a uniform temperature. In the case of rotary desorbers and kilns, however, several studies have suggested that the wall surface temperature may vary significantly as the wall is alternately covered by the solids bed and exposed to the freeboard gases [12, 49, 50]. That is, as the wall, which has a finite heat capacity, exchanges heat with the solids bed, its surface temperature will, in general, change. Thus, a boundary condition that assumes the wall to be isothermal may not always be appropriate.

PROBLEM FORMULATION, ANALYSES AND SOLUTIONS

From the review of existing literature, it is apparent that a number of important considerations are relevant to the problem at hand. However, all of these considerations have yet to be incorporated into a single analysis which describes heat transfer between a rotating cylinder wall and an adjacent moist granular bed. The model described in this paper calculates the wall-to-bed heat transfer rate and the moisture evaporation rate resulting from this heat transfer, while considering the following:

(1) the bed motion commonly encountered in rotary desorbers;

(2) the transport of energy via the flow of water vapor generated at the phase-change interface;

(3) the effects of bulk bed temperatures below the evaporation temperature of the moisture;

(4) the thermal contact resistance between the wall and immediately adjacent particles;

(5) a time-varying wall temperature.

In this way, the important features of wall-to-bed heat

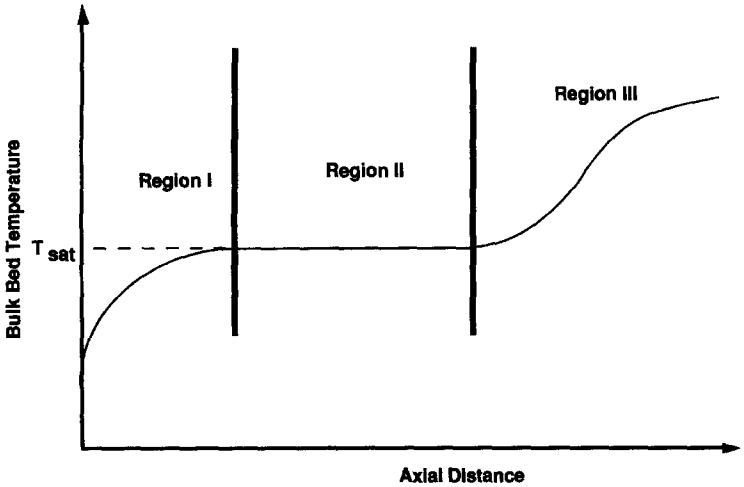

Fig. 3. Axial regions of the desorber and a hypothetical axial temperature profile.

transfer in a rotating cylinder are included in a single model.

Description of axial regions

In describing the wall-to-bed heat transfer model, it is helpful to consider three axial regions in the rotary desorber. These are illustrated in Fig. 3, which shows the general characteristics of the bulk solids temperature, T_b, as the solids move axially through the rotating cylinder. In the first axial region, Region I, the solids bed contains moisture and the bulk bed temperature is less than the saturation temperature of the moisture, T_{sat}. Even though the bulk of the bed is at a temperature less than the saturation temperature, the temperature of the bed near the hot wall may be greater than T_{sat}, and so some evaporation of water is possible in Region I. In Region II, the bed contains moisture, but the moisture is at saturation condition. All heat transferred to the bed in this axial region is assumed to evaporate moisture; there is assumed to be no sensible heating of the bed in Region II. Finally, in Region III it is assumed that there is no moisture remaining in the bed, and the bed is heated to temperatures above the saturation temperature. The division of the bed into these three axial regions is supported by the bed temperatures measured by Silcox and Pershing [11], Owens *et al.* [1], Walker [12], and Cook *et al.* [51]. In the following discussion, detailed wall-to-bed heat transfer models are developed for Regions I and II. Region III, which involves only dry solids, has been addressed in the literature [15, 18, 19, 52].

Region I problem formulation

The main objectives of the wall-to-bed heat transfer model are to calculate the heat transfer rate from the wall to the bed and the evaporation rate of water from the bed that results from this heat transfer. The model is developed first for an arbitrary axial location in Region I. The approach of the analysis in Region I is to develop and solve the governing equations in two layers within the bed at this axial location: a layer near the heated wall where no liquid remains (a dry layer containing only water vapor and dry solids), and a layer further from the wall which contains liquid. These two layers are separated by a phase-change interface. It is at this interface that the moisture in the bed is evaporated. The situation being modeled for Region I is shown in Fig. 4. In Fig. 4a, the actual geometry of the desorber cross-section is shown. In Fig. 4b, a cross-section of the bed near the wall is detailed. In Fig. 4b the curvature of the wall is neglected, and the dry layer near the wall and the phase-change interface are illustrated. The bed near the wall moves with the wall so that the bed moves with a uniform velocity relative to the fixed reference frame shown. Heat is conducted from the wall to the adjacent bed particles, and will be transported along the wall by the movement of the bed. In addition, energy will be transferred by the movement of the water vapor that is generated at the phase-change interface. In Region I, the following assumptions are made:

(1) the conditions (temperature and moisture content) of the solids when they contact the heated wall (at $x = 0$) are those of the well-mixed bulk bed;

(2) all evaporation and recondensation occur at the phase-change interface; thus there is assumed to be no flow of water vapor into the subcooled layer above the phase-change interface; any such vapor would be recondensed at the phase-change interface;

(3) all physical and thermal properties are constant with respect to temperature;

(4) the saturation temperature is assumed to correspond to the pressure inside the cylinder; since changes in the saturation pressure along the phase-change interface were determined to be small, the corresponding variations in the saturation temperature are neglected;

(5) the local temperature of the vapor phase is equal to that of the solid particles.

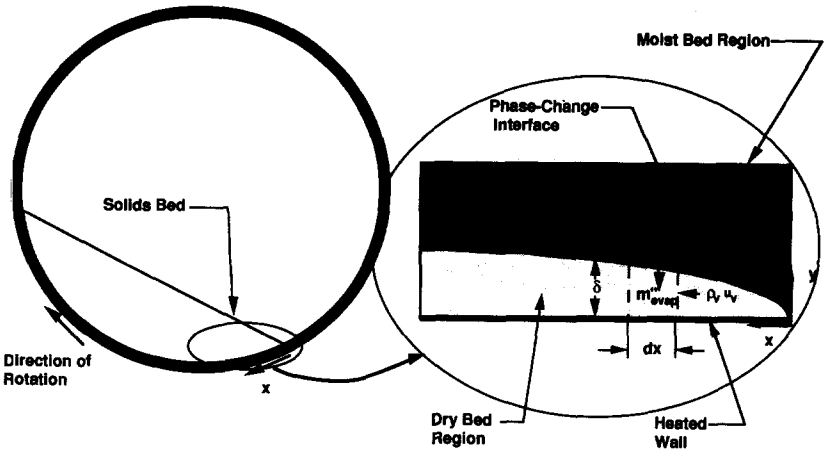

Fig. 4. Schematic diagram of the proposed wall-to-bed heat transfer model. (a) Actual bed geometry. (b) Assumed bed geometry near the heated wall.

The recondensation mentioned in assumption (2) may actually occur within a thin layer above the phase-change interface; however, if the water vapor is assumed to be in thermal equilibrium with the local solids (assumption 5), this recondensation layer collapses to a line at the phase-change interface. The phase-change interface provides the net rate of evaporation that satisfies the energy and mass balances developed below. Assumption (5) is supported by several studies [53–55]. For systems in which a gas is flowing through a bed of solids, it can be assumed that the vapor instantaneously reaches thermal equilibrium with the solids particles that it contacts. This assumption is justified by comparing the thermal time constants of the solids and the gas. Due to the large thermal capacitance of the solids relative to that of the gas phase, the time constant of the vapor is much less than that of the solid particles. Thus, the vapor will quickly approach the local temperature of the solids.

In the following discussion the approximate equations governing the flow of vapor in Region I are solved. Thus result is then incorporated into the governing energy equation, which will be solved to find the heat transfer rate from the wall to the bed for Region I.

The equations governing the transport of momentum in the vapor region adjacent to the wall can be approximated by Darcy's law and the continuity equation [45]:

$$\frac{\nu_v}{K}\rho_v \bar{u}_v = -\nabla p \tag{1}$$

$$\nabla \cdot \rho_v \bar{u}_v = 0 \tag{2}$$

where $\bar{u}_v$ is the Darcy velocity of the water vapor, K is the permeability of the dry solids bed, and ρ_v and ν_v are the density and kinematic viscosity of the vapor, respectively. Combining these equations under the assumption of constant properties gives

$$\nabla^2 p = 0. \tag{3}$$

Since the length scale in the y-direction (the thickness of the vapor region) is much less than the length scale in the x-direction, equation (3) may be approximated as

$$\frac{d^2 p}{dy^2} = 0. \tag{4}$$

The boundary conditions are

$$\left(\frac{dp}{dy}\right)_{y=0} = 0 \tag{5}$$

$$p(y = \delta) = p_{sat} \tag{6}$$

where p_{sat} is the pressure at the phase-change interface and δ is the thickness of the dry layer. The first boundary condition results from the impermeable wall. The solution to equation (4) with these boundary conditions is

$$p = p_{sat}. \tag{7}$$

Thus the solution to Darcy's equation predicts that the pressure in the vapor region is not a function of y and that the flow of vapor in the x-direction is uniform (not a function of y).

The x-direction vapor mass flow rate can be determined by first finding the rate at which vapor leaves the phase-change interface. This is done using a mass balance at the interface between the liquid and vapor regions. Similar mass balances are used in the analyses of Rubin and Schweitzer [44], Parmentier [45], Cheng [48], Cheng and Verma [46], and Essome and Orozco [47] in the study of phase change processes in static, porous media. In the present model, this interface

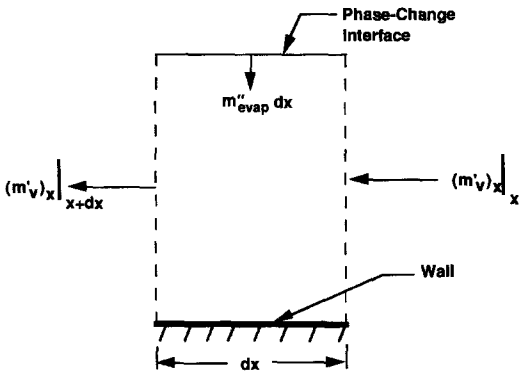

Fig. 5. Mass balance on vapor in the dry layer.

mass balance provides the flux of water vapor generated, m''_{evap}, at the interface:

$$m''_{evap} = \rho'_L u_s \frac{d\delta}{dx} \tag{8}$$

where ρ'_L is the mass of liquid per unit volume of the bed, and $d\delta/dx$ is the rate of growth of the dry layer. The speed of the solids moving with the wall, u_s, is given by $\omega\pi D$, where ω is the desorber rotation rate and D is the desorber diameter.

Now consider a mass balance on a differential length of the dry layer, as shown in Fig. 5. This mass balance yields

$$\frac{d(m'_v)_x}{dx} = m''_{evap} \tag{9}$$

where $(m'_v)_x$ is the mass flow rate in the x-direction per unit length of the desorber. From equations (8) and (9),

$$\frac{d(m'_v)_x}{dx} = \rho'_L u_s \frac{d\delta}{dx}. \tag{10}$$

Integrating equation (10) with the condition that the mass flow rate of vapor is zero when the vapor thickness, δ, is zero gives the mass flow rate of vapor in the dry layer per unit length of the desorber,

$$(m'_v)_x = \rho'_L u_s \delta. \tag{11}$$

Dividing this result by the local thickness of the dry layer, δ, gives the local mass flux of vapor, $\rho_v u_v$, in this layer,

$$\rho_v u_v = \frac{(m'_v)_x}{\delta} = \rho'_L u_s. \tag{12}$$

Note that the vapor mass flux given by equation (12) is constant. Equation (12) also allows the Darcy velocity in the dry layer to be estimated. For example, assuming a bulk bed density of 1230 kg m^{-3}, a vapor phase density of 0.46 kg m^{-3}, a wall speed of 0.032 m s^{-1} (a 0.61 m diameter drum rotating at 1 rpm), and a 5% water mass fraction (based on the mass of dry solids) yields a vapor Darcy velocity of 4.3 m s^{-1}.

Knowing the mass flux of vapor near the wall, the heat transfer in this region (including heat transfer resulting from the flow of vapor) can be determined. An energy equation can be written for a fixed control volume adjacent to the wall through which solids and vapor flow. This energy equation must include the convection of energy due to the movement of the bed, the convection of energy in the x-direction by the water vapor generated at the interface, and the conduction of heat in the direction normal to the heated wall,

$$(1-\varepsilon)u_s\rho_p c_p \frac{\partial T}{\partial x} + \rho_v u_v c_v \frac{\partial T}{\partial x} = k_s \frac{\partial^2 T}{\partial y^2} \tag{13}$$

where T is the local temperature in the dry layer, $\rho_v u_v$ is the mass flux of vapor with respect to the fixed reference frame, u_v is the Darcy velocity of the vapor in the x direction, c_p is the specific heat of the solid particles, k_s is the thermal conductivity of the dry layer, ε is the bed porosity, and ρ_p is the density of the particles. Conduction in the x-direction is neglected.

The derivative with respect to the fixed coordinate, x, in equation (13) can be replaced by a time derivative using the following relation:

$$x = u_s t \tag{14}$$

where t is the time for which a particle at location x has been in contact with the rotating wall. The energy equation then becomes

$$\frac{\partial T}{\partial t}\left((1-\varepsilon)\rho_p c_p + \frac{\rho_v u_v c_v}{u_s}\right) = k_s \frac{\partial^2 T}{\partial y^2}. \tag{15}$$

Defining

$$\alpha_e = \frac{k_s}{(1-\varepsilon)\rho_p c_p + \rho'_L c_v} \tag{16}$$

gives

$$\frac{\partial \theta}{\partial t} = \alpha_e \frac{\partial^2 \theta}{\partial y^2} \tag{17}$$

where $\theta = T - T_{sat}$. Substituting equation (12) into equation (16) gives

$$\alpha_e = \frac{k_s}{(1-\varepsilon)\rho_p c_p + \rho'_L c_v}. \tag{18}$$

Note that, under the assumption of constant properties, α_e is constant.

Region I analysis and solution

The governing equation to be solved for Region I is given by equation (17). If no thermal contact resistance existed at the wall and the wall temperature was assumed to be constant, the problem would be analogous to the classical Nuemann problem [2]. To include the effects of a thermal contact resistance at the wall and a circumferentially varying wall temperature, however, equation (17) must be solved with the following initial and boundary conditions:

$$\delta(t = 0) = 0 \tag{19}$$

$$-k_s\left(\frac{\partial\theta}{\partial y}\right)_{y=0} = h_c(\theta_w(t)-\theta_{y=0}) \tag{20}$$

$$\theta(\delta, t) = 0 \tag{21}$$

where $\theta_w = T_w - T_{sat}$, T_w is local temperature of the rotating wall, and h_c is the heat transfer coefficient describing the thermal contact resistance between the wall and adjacent particles.

Since no exact analytical solution exists to this problem, an integral solution method was applied. The integral solution method requires an assumed form for the bed temperature profile in the y-direction. In the present model, the heat-balance integral method with a parabolic temperature profile between the wall and the phase-change interface is used to solve equation (17) with the conditions of equations (19)–(21). Cook [2] has shown that the second-order polynomial approximation introduces errors in the wall-to-bed heat flux of less than 5%.

Integrating equation (17) over the dry layer thickness, δ, gives

$$\frac{d}{dt}\int_0^{\delta}\theta\,dy = \alpha_e\left[\left(\frac{\partial\theta}{\partial y}\right)_{y=\delta} - \left(\frac{\partial\theta}{\partial y}\right)_{y=0}\right]. \tag{22}$$

In the following discussion, the two bracketed terms on the right-hand-side of equation (22) are determined. The second term follows from the form of the temperature assumed for the dry layer, while the first term is found by considering an energy balance at the phase-change interface.

The parabolic temperature profile assumed for $0 < y < \delta$ is

$$\theta = a(y-\delta)+b(y-\delta)^2 \tag{23}$$

where a and b are coefficients that must be determined. With this profile, the second term on the right-hand side of equation (22) can be directly evaluated,

$$\left(\frac{\partial\theta}{\partial y}\right)_{y=0} = a-2b\delta. \tag{24}$$

In order to evaluate the first term on the right-hand side of equation (22), an energy balance at the phase-change interface must be considered. In Region I, the interface energy balance must account for the fact that the bulk temperature is less than the temperature of the moving interface. Heat will be conducted from the interface to the moist bed; thus, not all of the heat conducted to the interface will vaporize moisture. The interface energy balance at a location in Region I is then

$$-k_s\left(\frac{\partial\theta}{\partial y}\right)_{y=\delta} = XH_v\rho_s\frac{\partial\delta}{\partial t} - k_m\left(\frac{\partial\theta_m}{\partial y}\right)_{y=\delta} \tag{25}$$

where H_v is the heat of vaporization of water, X is the mass fraction of water in the moist region, and ρ_s is the bulk density of the dry solids bed. The subscript m represents properties and conditions of the moist bed above the phase-change interface, and θ_m is the temperature profile in the moist region, where $\theta_m = T_m - T_{sat}$. Using equation (25), the first term on the right-hand side of equation (22) is obtained,

$$\left(\frac{\partial\theta}{\partial y}\right)_{y=\delta} = -A\frac{\partial\delta}{\partial t} - \frac{k_m}{k_s}\left(\frac{\partial\theta_m}{\partial y}\right)_{y=\delta} \tag{26}$$

where

$$A = \frac{XH_v\rho_s}{k_s}. \tag{27}$$

However, equation (26) cannot be applied until the temperature profile in the moist region, θ_m, is known. To find this profile, the transient energy equation for the moist region was solved using a heat-balance integral method. The governing equations, initial condition, and boundary conditions for the moist region are as follows:

$$\frac{\partial\theta_m}{\partial t} = \alpha_m\frac{\partial^2\theta_m}{\partial y^2} \tag{28}$$

$$\delta_m(t=0) = 0 \tag{29}$$

$$\theta_m(\delta, t) = 0 \tag{30}$$

$$\theta_m(\infty, t) = \theta_b \tag{31}$$

where δ_m is the thickness of the thermal layer beyond which there is no change in temperature with respect to y, and $\theta_b = T_b - T_{sat}$. Equation (28) is integrated from $y = \delta$ to $y = \delta_m$ using the rule of Leibnitz. The result is

$$\frac{d}{dt}\int_{\delta}^{\delta+\delta_m}\theta_m\,dy - \theta_b\frac{d(\delta+\delta_m)}{dt} = \alpha_m\left(\frac{\partial\theta_m}{\partial y}\right)_{y=\delta+\delta_m} - \alpha_m\left(\frac{\partial\theta_m}{\partial y}\right)_{y=\delta}. \tag{32}$$

A second-order temperature profile is assumed for $\delta < y < \delta_m$ that satisfies the following conditions:

$$\theta_m(\delta, t) = 0 \tag{33}$$

$$\theta_m(\delta+\delta_m, t) = \theta_b \tag{34}$$

$$\left(\frac{\partial\theta_m}{\partial y}\right)_{y=\delta+\delta_m} = 0. \tag{35}$$

The resulting profile for the moist region is

$$\theta_m = 2\theta_b\left(\frac{y-\delta}{\delta_m}\right) - \theta_b\left(\frac{y-\delta}{\delta_m}\right)^2. \tag{36}$$

Substituting this profile into the heat-balance integral for the moist region, equation (32), gives the following ordinary differential equation for δ_m:

$$\frac{d\delta_m}{dFo} = \frac{k_s}{h_c}\frac{d\Delta}{dFo}\left(-3+3A\frac{\alpha_m k_s}{\theta_b k_m}\right)+3a\frac{\alpha_m k_s}{\alpha_e k_m\theta_b}\left(\frac{k_s}{h_c}\right)^2. \tag{37}$$

In equation (37), the following dimensionless parameters have been introduced:

$$Fo = \frac{\alpha_e t}{\left(\frac{k_s}{h_c}\right)^2} \tag{38}$$

$$\Delta = \frac{\delta h_c}{k_s}. \tag{39}$$

Knowing δ_m by integrating equation (37), the moist bed temperature profile, θ_m, is obtained from equation (36) and the required term in equation (22) can be directly calculated,

$$\left(\frac{\partial \theta_m}{\partial y}\right)_{y=\delta} = \frac{2\theta_m}{\delta_m}. \tag{40}$$

Substituting equations (26) and (40) into the heat-balance integral for the dry layer, equation (22), gives

$$\frac{d}{dt}\int_0^\delta \theta \, dy = \alpha_e\left[-A\frac{d\delta}{dt} + \frac{k_m}{k_e}\frac{2\theta_b}{\delta_m} - (a-2b\delta)\right]. \tag{41}$$

To evaluate the integral in equation (41), the temperature profile, θ, must be determined. The coefficients of the temperature profile, equation (23), are determined by the condition given by equation (20) and the interface energy balance [2, 56, 57]. The results are

$$a = \frac{h_c\alpha_e A(1+\Delta)}{\Delta(2+\Delta)k_s} + \frac{k_m\theta_b}{\delta_m k_s} - \frac{1}{2}\sqrt{\left[\frac{2h_c\alpha_e A(1+\Delta)}{\Delta(2+\Delta k_s} + \frac{2k_m\theta_b}{\delta_m k_s}\right]^2 + \frac{8h_c^2\alpha_e A\theta_w}{k_s^2\Delta(2+\Delta)}} \tag{42}$$

and

$$b = \frac{a^2}{2\alpha_e A} - \frac{k_m\theta_b a}{k_e\delta_m\alpha_e A}. \tag{43}$$

With these coefficients, equation (41) yields a differential equation for the interface location:

$$\frac{d\Delta}{dFo} = \frac{\left(\frac{\partial a}{\partial\theta_w}\frac{d\theta_w}{dFo} + \frac{\partial a}{\partial\delta_m}\frac{d\delta_m}{dFo}\right)\left(\frac{\Delta^2}{2} - \frac{\Delta^3}{3}\frac{k_s}{h_c}\frac{\partial b}{\partial a}\right) - \frac{\Delta^3}{3}\frac{k_s}{h_c}\frac{\partial b}{\partial\delta_m}\frac{d\delta_m}{dFo} - a + 2b\frac{k_s}{h_c}\Delta + \frac{2\theta_b k_m}{\delta_m k_e}}{-a\Delta + b\Delta^2\frac{k_s}{h_c} - \frac{1}{2}\Delta^2\frac{\partial a}{\partial\Delta} + \frac{1}{3}\Delta^3\frac{k_s}{h_c}\frac{\partial b}{\partial a}\frac{\partial a}{\partial\Delta} + A\alpha_e\left(\frac{h_c}{k_s}\right)} \tag{44}$$

where

$$\frac{\partial a}{\partial\theta_w} = \frac{h_c^2\alpha_e A}{ak_s^2\Delta(2+\Delta) - k_s h_c\alpha_e A(1+\Delta) - \frac{k_s k_m\theta_b\Delta(2+\Delta)}{\delta_m}} \tag{45}$$

$$\frac{\partial a}{\partial\delta_m} = \frac{ak_m\theta_b\Delta(2+\Delta)}{-a\delta_m^2 k_s\Delta(2+\Delta) + \delta_m^2 h_c\alpha_e A(1+\Delta) + k_m\theta_b\delta_m\Delta(2+\Delta)} \tag{46}$$

$$\frac{\partial a}{\partial\Delta} = \frac{a\left[\frac{2h_c\alpha_e A}{k_s}\frac{\Delta(2+\Delta)-2(1+\Delta)^2}{\Delta^2(2+\Delta)^2}\right] - \frac{4h_c^2\alpha_e A\theta_w(1+\Delta)}{k_e^2\Delta^2(2+\Delta)^2}}{2a - \frac{2h_c\alpha_e A(1+\Delta)}{k_s\Delta(2+\Delta)} - \frac{2k_m\theta_b}{\delta_m k_s}} \tag{47}$$

$$\frac{\partial b}{\partial a} = \frac{a}{\alpha_e A} - \frac{k_m\theta_b}{k_s\delta_m\alpha_e A} \tag{48}$$

and $d\theta_w/dFo$ is the specified dimensionless wall temperature gradient. Using the initial condition of equation (19), equation (44) can be numerically integrated to give Δ as a function of Fo. The quantity $d\delta_m/dFo$ is given by equation (37), which must be solved simultaneously with equation (44) in order to determine δ_m.

With Δ known at a given value of Fo, several useful quantities can be determined. The instantaneous heat flux from the wall to the bed is

$$q''_{w-b} = k_s\left(a - 2b\frac{\Delta k_s}{h_c}\right) \tag{49}$$

where a and b are given by equations (42) and (43). Equation (49) is integrated over the contact time, the time a bed particle is in contact with the wall, to obtain the average wall-to-bed heat flux at an axial location in Region I.

The local flux of water vapor generated at the interface is

$$m''_{evap} = X\rho_s u_s\frac{d\delta}{dx}. \tag{50}$$

This mass flux is numerically integrated over the length of the covered wall to find the overall evaporation rate per unit length of the desorber at the axial location under consideration.

Special case: *bed temperature at wall less than saturation temperature.* The solution represented by equation (49) assumes that the temperature at $y = 0$ is at least the saturation temperature of the moisture, so that moisture can be vaporized. However, due to the thermal contact resistance at the wall, this temperature may be less than T_{sat}, even if the wall temperature is greater than T_{sat}. In this case, no evap-

oration occurs, and heat is simply conducted through the thermal contact resistance and into the moist bed. An integral method has also been used to solve this case, and the resulting wall-to-bed heat flux is as follows:

$$q''_{w\text{-}b} = k_m(a-2b\delta_m) \tag{51}$$

where

$$a = 0 \tag{52}$$

$$b = \frac{h_c\theta_w}{h_c\delta_m^2+2k_m\delta_m}. \tag{53}$$

In this case, the following differential equation governs the growth of the thermal penetration layer into the moist bed:

$$\frac{d\delta_m}{dFo} = \frac{\dfrac{2\alpha_m}{\delta_m} - \dfrac{\delta_m h_c^3}{k_m^2}\dfrac{\alpha_m}{}\dfrac{d\theta_w}{dFo}\dfrac{(h_c\delta_m^2+2k_m\delta_m)}{3b(h_c\delta_m^2+2k_m\delta_m)^2}}{\dfrac{\alpha_m h_c^2}{\delta_m}\left[1-\dfrac{2(\theta_w h_c^2\delta_m^2+k_m h_c\theta_w\delta_m)}{3b(h_c\delta_m^2+2k_m\delta_m)^2}\right]}. \tag{54}$$

Region II problem formulation

A similar analysis can be made for Region II. However, several characteristics of this axial region produce a solution which is simpler than that of Region I. Recall that in Region II the bulk of the bed is at the saturation temperature of the moisture. Thus the liquid is saturated, and, if the entire pore volume is not filled with liquid, saturated vapor may exist in the remaining pore volume. If this is the case, some of the vapor generated at the interface may flow through this volume, reducing the vapor flow along the heated surface. As noted by Schlünder and Mollekopf [39], the mass transfer resistance through the moist bed is usually low, so that essentially all of the vapor generated at the interface will take this path when the bulk bed temperature is equal to the phase-change temperature. In this case, the governing equation, equation (17), must be solved with $\alpha_e = \alpha_s$. That is, with no vapor flow in the dry layer, the effective thermal diffusivity reduces to that of the dry layer. With the bulk bed temperature equal to the phase-change temperature, the phase-change interface energy balance also simplifies. There is no longer conduction of heat from the phase-change interface to the bulk of the bed. These simplifications are demonstrated in the following analysis.

Region II analysis and solution

Similar to Region I, a heat-balance integral method was used to find a solution to the governing transient heat conduction equation with a thermal contact resistance boundary condition at the wall. If the wall temperature is constant, the integral solution for Region II yields a closed form solution [56, 57]. A more general case can be considered by allowing the wall temperature to vary with time. This case is considered in the following analysis.

The governing energy equation is given by equation (17), and the initial and boundary conditions are given by equations (19)–(21). The heat-balance integral is found by integrating equation (17) over the dry layer,

$$\frac{d}{dt}\int_0^\delta \theta\,dy = \alpha_e\left[\left(\frac{\partial\theta}{\partial y}\right)_{y=\delta} - \left(\frac{\partial\theta}{\partial y}\right)_{y=0}\right]. \tag{55}$$

As in Region I, the evaluation of the two bracketed terms on the right-hand side of equation (55) is required. The first term is found from the interface energy balance,

$$\left(\frac{\partial\theta}{\partial y}\right)_{y=\delta} = -A\frac{\partial\delta}{\partial t}. \tag{56}$$

Assuming a parabolic temperature profile for the dry layer,

$$\theta = a(y-\delta)+b(y-\delta)^2 \tag{57}$$

yields

$$\left(\frac{\partial\theta}{\partial y}\right)_{y=0} = a-2b\delta. \tag{58}$$

Substituting equations (56) and (58) into the heat-balance integral, equation (55), gives

$$\frac{d}{dt}\int_0^\delta \theta\,dy = \alpha_e\left[-A\frac{d\delta}{dt}-(a-2b\delta)\right]. \tag{59}$$

Again, the coefficients of the temperature profile are determined by the condition of equation (20) and the interface energy balance, equation (56). The results for Region II are

$$a = \frac{(1+\Delta)-\sqrt{(1+\Delta)^2+\dfrac{2\theta_w}{\alpha_e A}\Delta(2+\Delta)}}{\dfrac{k_s\Delta(2+\Delta)}{\alpha_e A h_c}} \tag{60}$$

and

$$b = \frac{a^2}{2\alpha_e A}. \tag{61}$$

With these coefficients, equation (59) yields a differential equation for the interface location:

$$\frac{d\Delta}{dFo} = \frac{\left[\frac{1}{2}\Delta^2-\frac{1}{3}\left(\frac{k_s}{h_c}\right)\Delta^3\frac{a}{\alpha_e A}\right]\frac{\partial a}{\partial\theta_w}\frac{d\theta_w}{dFo}-a+2b\left(\frac{k_s}{h_c}\right)\Delta}{-a\Delta+b\Delta^2\left(\frac{k_s}{h_c}\right)+\left(\frac{h_c}{k_s}\right)\alpha_e A-\frac{\partial a}{\partial\Delta}\left(\frac{1}{2}\Delta^2-\frac{1}{3}\left(\frac{k_s}{h_c}\right)\Delta^3\frac{a}{\alpha_e A}\right)}. \tag{62}$$

From equations (60) and (61) the following quantities are determined:

$$\frac{\partial a}{\partial \Delta} = \frac{-a^2 \dfrac{k_s}{\alpha_e A h_c}(1+\Delta)+a}{a\dfrac{k_s}{\alpha_e A h_c}\Delta(2+\Delta)-(1+\Delta)} \tag{63}$$

and

$$\frac{\partial a}{\partial \theta_w} = -\left(\frac{h_c}{k_s}\right)\left[(1+\Delta)^2+\frac{2\theta_w}{\alpha_e A}\Delta(2+\Delta)\right]^{-3/2} \tag{64}.$$

Using the initial condition of equation (19), equation (62) can be numerically integrated to give Δ as a function of Fo. With Δ known at a given value of Fo, the heat flux from the wall to the bed is

$$q''_{w\text{-}b} = k_s\left(a-2b\frac{\Delta k_s}{h_c}\right) \tag{65}$$

where a and b are given by equations (60) and (61). Equation (65) is integrated over the contact time to obtain the total wall-to-bed heat transfer rate at any axial location. Since there is assumed to be no sensible heating in Region II, all of the heat transferred to the bed yields evaporation of water.

RESULTS AND MODEL VALIDATION

To demonstrate the validity and usefulness of the wall-to-bed heat transfer model described in this paper, predictions of the model were compared to experimental data. These experimental data were taken from a batch-type, pilot-scale rotary desorber with an internal diameter of 0.61 m and a length of 0.61 m. Unlike continuously fed desorbers, the experimental facility operates in a batch mode. That is, materials do not continuously pass through the cylinder; when materials are introduced to the unit, they remain there until they are manually removed. Measuring the transient response of the charge in this batch-type unit is equivalent to monitoring a charge of material as it moves along the axis of a continuously fed rotary desorber. In the experiments, charges of wet sand were introduced into the test section of the desorber. Heat was transferred to the solids from the rotating desorber wall and from hot combustion gases passing over the exposed surface of the solids bed. Both the rotating wall and the gas phase were at a temperature of approx. 300°C. The transient temperature of the solids bed was measured at several locations by thermocouples placed within the bed. A typical bulk bed temperature profile is displayed in Fig. 6, where the three periods corresponding to the three axial regions of Fig. 3 are clearly shown. As indicated previously, the prediction of the water evaporation rate is of critical importance in predicting the bed temperature profiles. The evaporation rate was determined experimentally by measuring the velocity of the gas leaving the exit duct of the pilot-scale desorber. Using this velocity and the locally-measured temperature, the mass flow rate of gas leaving the desorber was calculated. By subtracting the baseline

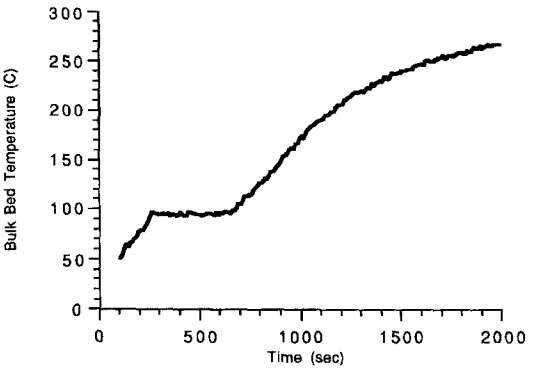

Fig. 6. Typical experimentally measured bulk bed temperature profile.

mass flow rate (determined when no evaporation was occurring) from the total mass flow rate with evaporation, the instantaneous water evaporation rate was determined. Experiments were performed at two rotation rates: 1.0 and 2.0 rpm. Details of these experiments are described in Cook *et al.* [51], along with a complete discussion of the results.

The heat transfer model requires input parameters which specify the operating conditions during each experiment. The following parameters, which were measured during the experiments, were specified as input values for the model: the transient wall temperature, the initial temperature of the solids, the initial mass fraction of the water in the charge, and the wall rotation rate. The specific heat and the bulk density of the solids bed and the density of the bed particles were determined by independent experiments [51], and were used as input parameters to the model. In addition, the correlation of Krupiczka [58] was used to estimate the thermal conductivities of the solids bed. The required bulk bed temperature was calculated using the model of Cook [2].

As mentioned previously, the thermal contact resistance between the wall and the first layer of particles is a function of particle size and shape, particle and surface roughnesses, and interstitial gas properties. Since the particles used in the experiments are angular and non-spherical, the expression derived by Malhotra and Mujumdar [27] for slab-shaped particles was used to calculate the contact heat transfer coefficient,

$$h_c = \frac{\sqrt{2}k_v}{D_p}\ln\left[\frac{D_p\sqrt{2}}{2(\sigma+s_r)}+1\right] \tag{66}$$

where k_v is the conductivity of the interstitial water vapor evaluated at the average of the wall and saturation temperature, D_p is the length of one side of the particle, σ is the reduced mean molecular free path, and s_r is the sum of the roughnesses of the particles and wall. Following the recommendation of Schlünder [25], s_r is assumed to be zero. The effects of this thermal contact resistance on wall-to-bed heat transfer are discussed by Cook [2].

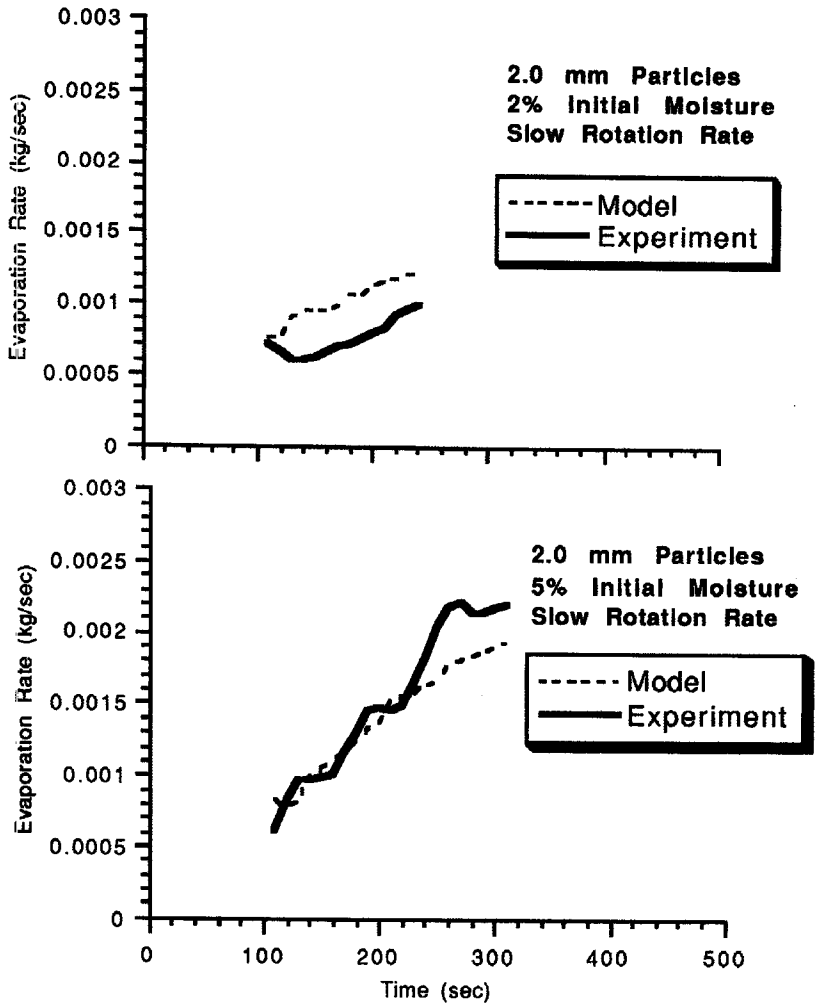

Fig. 7. Comparison of predicted and measured evaporation rates for bulk bed temperatures below the water saturation temperature: slow rotation rate.

Of particular interest is the evaporation of moisture before the bulk bed temperature reaches the saturation temperature of the moisture. Recall that previous models have neglected evaporation under these conditions. In the following discussion, these experimentally measured evaporation rates are compared to those predicted by the model for Region I (bulk bed temperatures below the water saturation temperature).

Figures 7 and 8 compare the experimentally determined evaporation rates with those predicted by the model for the time period corresponding to Region I. Results are shown for both rotation rates and for three initial moisture fractions: 2, 5, and 7% mass. In Fig. 7, the results for an initial moisture content of 7% are not shown, since the bed motion under these conditions was inconsistent with that assumed by the model. Figures 7 and 8 show that both the predicted and measured evaporation rates increase with time. This increase occurs simultaneously with an increasing bulk bed temperature, as shown in Fig. 6. Given the uncertainty in experimental measurement and parameter estimation, the agreement between model and experimental data is remarkably good. It is noted, however, that the evaporation rate is over-predicted for the 2% initial moisture content cases, and is under-predicted for the 5% and 7% initial moisture content cases.

Further comparisons can be made between the experimental and model results by considering the total mass of water evaporated before the bed reaches the saturation temperature (Region I). This quantity was calculated both from the experimental data and from the model predictions, and the results are shown in Table 1. These results demonstrate the importance of evaporation at bulk temperatures below the moisture saturation temperature; the experimental results show that 25–40% of the initial water mass evaporates before the bed reaches the saturation temperature. At the slower rotation rate with an initial moisture content of 2%, the model over-predicts the total mass of water evaporated in this region by 43%, relative to the experimental data. For the remaining four cases, the total mass evaporated before the bulk bed tem-

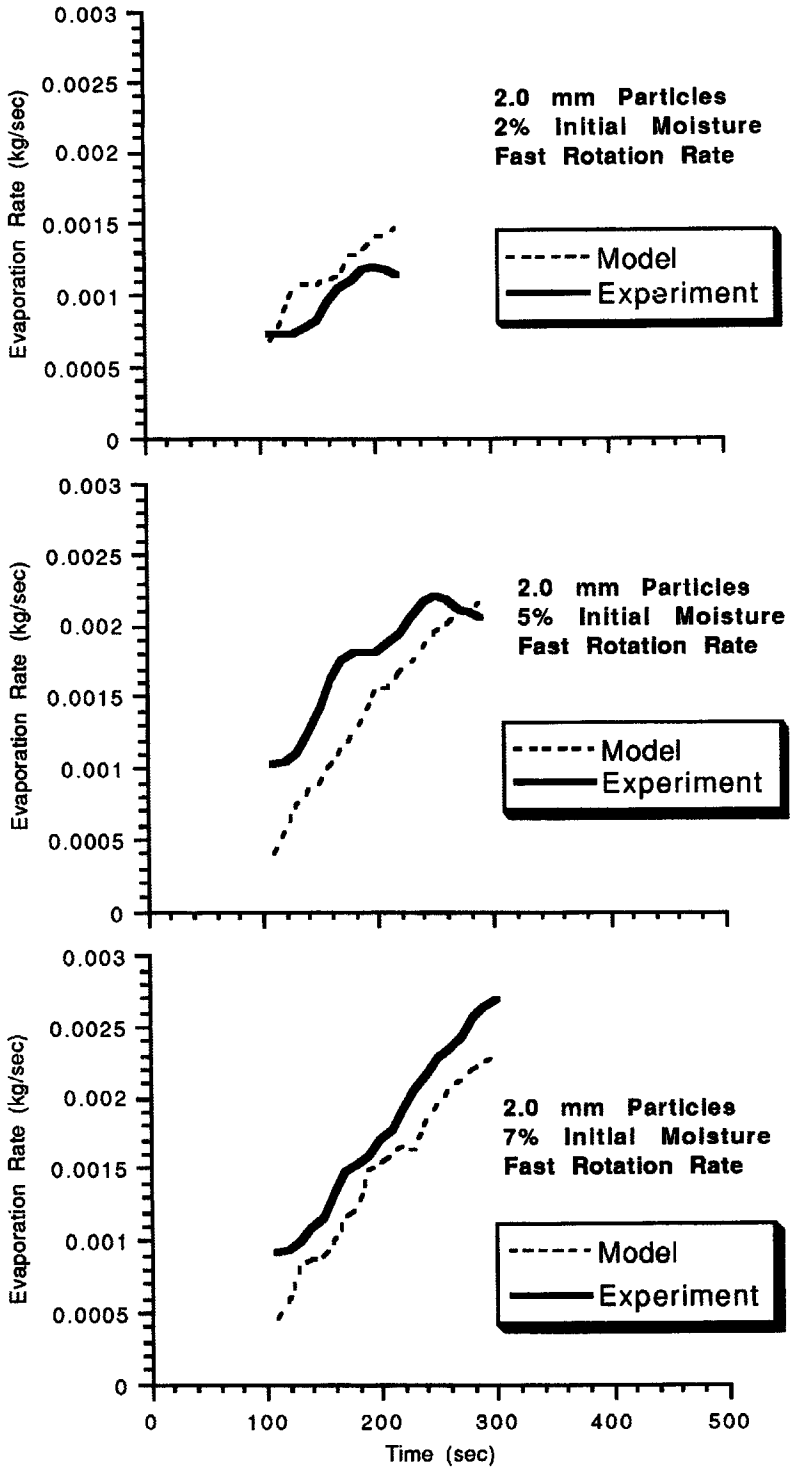

Fig. 8. Comparison of predicted and measured evaporation rates for bulk bed temperatures below the water saturation temperature: fast rotation rate.

perature reaches the water saturation temperature is predicted to within 22% of the experimental results. Again, both the experimental data and the model show that moisture evaporation in Region I can be significant under certain conditions. The relatively good agreement between experimental data and the model shows that the model accurately describes this important evaporation process. Also, the wall-to-bed heat transfer model described in this paper has been used in a comprehensive heat transfer model (which

Table 1. Comparison of experimental and predicted water evaporation for bulk bed temperatures below T_{sat} (Region I)

Initial moisture content	Rotation rate (rpm)	Percentage of initial water mass evaporated	
		Experimental	Model prediction
2%	1.0	39.8	56.9
5%	1.0	31.7	30.6
2%	2.0	37.5	44.4
5%	2.0	30.9	24.1
7%	2.0	24.7	21.7

includes the heat transfer mechanisms involving the exposed surface of the bed) to predict changes in the bulk bed temperature [2], resulting in axial temperature profiles which agree well with those found experimentally for Region I. This agreement suggests that the wall-to-bed heat transfer model can accurately predict the sensible heating of the solids bed as well as the evaporation rate from the bed in this region.

SUMMARY AND CONCLUSIONS

An analytical model has been developed to predict heat and mass transfer phenomena in a wet porous medium near a heated rotating surface. A heat-balance integral method is used to model heat conduction from the wall to adjacent wet bed particles. This solution includes the effects of water evaporation near the wall and a thermal contact resistance between the wall and the first layer of particles. The model allows for water evaporation before the bulk bed temperature reaches the saturation temperature of the water. A simplified heat transfer model is also presented for the case where the bulk bed temperature is at the moisture saturation temperature.

Experimental results show that evaporation before the bulk bed temperature reaches the water saturation temperature may, at times, be significant. The evaporation rates for this region that are predicted by the model agree well with experimental measurements. Thus, for the first time, it is possible to predict moisture evaporation before the bulk temperature reaches the saturation temperature (Region I). Since the water evaporation rate can significantly affect the temperature history of the solids, this ability may greatly improve more comprehensive models that predict temperature profiles throughout the desorber. Ultimately, this will improve predictions of contaminant desorption, since the contaminant desorption rate is determined primarily by the temperature-dependent partitioning between the contaminant and the soil particles.

Acknowledgements—The research described in this article has been funded in part by Chemical Waste Management, Inc. through the Hazardous Waste Research Center of the Louisiana State University. However, it has not been subjected to company review and no official endorsement should be inferred. The support offered by Dr L. J. Thibodeaux and Dr David Constant, Director and Associate Director, respectively, of the Louisiana State University Hazardous Waste Research Center, is appreciated. The assistance of the Advanced Combustion Engineering Research Center at the University of Utah is acknowledged. In particular, the assistance of Dr David W. Pershing, Dr JoAnn S. Lighty, Dr Fred S. Larsen, and Mr David Wagner is appreciated. The authors also gratefully acknowledge the fellowship assistance from the State of Louisiana for Charles A. Cook.

REFERENCES

1. W. D. Owens, G. D. Silcox, J. S. Lighty, X. X. Deng, D. W. Pershing, V. A. Cundy, C. B. Leger and A. L. Jakway, Thermal analysis of rotary kiln incineration: comparison of theory and experiment, *Combust. Flame* **86,** 101–114 (1991).
2. C. A. Cook, A study of heat transfer in rotary desorbers used to remediate contaminated soils, Ph.D. Dissertation, Louisiana State University (1993).
3. J. S. Lighty, D. W. Pershing, V. A. Cundy and D. G. Linz, Characterization of thermal desorption phenomena for the cleanup of contaminated soil, *Nucl. Chem. Waste Mgmt* **8,** 225–237 (1988).
4. J. S. Lighty, G. D. Silcox, D. W. Pershing, V. A. Cundy and D. G. Linz, Fundamental experiments on thermal desorption of contaminants from soils, *Envir. Prog.* **8,** 57–61 (1989).
5. J. S. Lighty, G. D. Silcox, D. W. Pershing, V. A. Cundy and D. G. Linz, Fundamentals for the thermal remediation of contaminated soils. Particle and bed desorption models, *Envir. Sci. Technol.* **24,** 750–757 (1990).
6. J. S. Lighty, E. G. Eddings, E. R. Lingren, X. X. Deng, D. W. Pershing, R. M. Winter and W. H. McClennen, Rate limiting processes in the rotary-kiln incineration of contaminated solids, *Combust. Sci. Technol.* **74,** 31–49 (1990).
7. C. Borkent-Verhage, C. Cheng, L. de Galan and E. W. B. de Leer, Thermal cleaning of soil contaminated with γ-hexachlorocyclohexane. In *Contaminated Soil* (Edited by J. W. Assink and W. J. van de Brink), pp. 883–886. Martinus Nijhoff, Dordrecht (1986).
8. C. P. Varuntanya, M. Hornsby, A. Chemburkar and J. W. Bozzelli, Thermal desorption of hazardous and toxic compounds from soil matrices. In *Petroleum Contaminated Soils*, Vol. 2 (Edited by E. J. Calabrese and P. T. Kostecki), pp. 251–265. Lewis, Chelsea, MI (1989).
9. L. Tognotti, M. Flytzani-Stephanopoulos, A. F. Sorofim, H. Kopsinis and M. Stoukides, Study of adsorption–desorption of contaminants on single soil particles using the electrodynamic thermogravimetric analyzer, *Envir. Sci. Technol.* **25,** 104–109 (1991).
10. A. Sass, Simulation of the heat-transfer phenomena in a rotary kiln, *Ind. Engng Chem. Process. Des. Dev.* **6,** 532–535 (1967).
11. G. D. Silcox and D. W. Pershing, The effects of rotary kiln operating conditions and design on burden heating rates as determined by a mathematical model of rotary kiln heat transfer, *J. Air Pollut. Control Ass.* **40,** 337–344 (1990).

12. D. A. Walker, The desorption of toluene in the presence of water in a rotary kiln environment, M.S. Thesis, University of Utah (1992).
13. R. Hogg and D. W. Fuerstenau, Transverse mixing in rotating cylinders, *Powder Technol.* **6,** 139–148 (1972).
14. G. W. J. Wes, A. A. H. Drinkenburg and S. Stemerding, Solids mixing and residence time distribution in a horizontal rotary drum reactor, *Powder Technol.* **13,** 177–184 (1976).
15. M. H. Lehmberg and K. Schugerl, Transverse mixing and heat transfer in horizontal rotary drum reactors, *Powder Technol.* **18,** 149–163 (1977).
16. H. Henein, J. K. Brimacombe and A. P. Watkinson, Experimental study of transverse bed motion in rotary kilns, *Metall. Trans.* **14B,** 191–205 (1983).
17. H. Henein, J. K. Brimacombe and A. P. Watkinson, The modeling of transverse solids motion in rotary kilns, *Metall. Trans.* **14B,** 207–220 (1983).
18. S. H. Tscheng and A. P. Watkinson, Convective heat transfer in a rotary kiln, *Can. J. Chem. Engng* **57,** 433–443 (1979).
19. G. W. J. Wes, A. A. H. Drinkenburg and S. Stemerding, Heat transfer in a horizontal rotary drum reactor, *Powder Technol.* **13,** 185–192 (1976).
20. S. Yagi and D. Kunii, Studies on heat transfer near wall surface in packed beds, *A.I.Ch.E. Jl* **6,** 97–104 (1960).
21. S. Yagi and D. Kunii, Radially effective thermal conductivities in packed beds, *Proceedings of the* 1961–1962 *Heat Transfer Conference*, pp. 750–759 (1962).
22. K. Ofuchi and D. Kunii, Heat-transfer characteristics of packed beds with stagnant fluids, *Int. J. Heat Mass Transfer* **8,** 749–757 (1965).
23. W. N. Sullivan and R. H. Sabersky, Heat transfer to flowing granular media, *Int. J. Heat Mass Transfer* **18,** 97–107 (1975).
24. E. U. Schlünder, Contact drying of particulate material under vacuum. In *Drying* '80, *Vol.* 1: *Developments in Drying* (Edited by A. S. Mujumdar), pp. 184–193. Hemisphere, Washington, DC (1980).
25. E. U. Schlünder, Particle heat transfer, *Proceedings of the 7th International Heat Transfer Conference*, Vol. 1, pp. 195–211. Hemisphere, New York (1982).
26. P. Richard and G. S. V. Raghavan, Particle–particle heat transfer applications to drying and processing—a review. In *Drying* '80, *Vol.* 1: *Developments in Drying* (Edited by A. S. Mujumdar), pp. 132–140. Hemisphere, Washington, DC (1980).
27. K. Malhotra and A. S. Mujumdar, Immersed surface heat transfer in a vibrated fluidized bed, *J. Chem. Engng Japan* **23,** 510–513 (1990).
28. K. Malhotra and A. S. Mujumdar, Model for contact heat transfer in mechanically stirred granular beds, *Int. J. Heat Mass Transfer* **34,** 415–425 (1991).
29. N. K. Harakas and K. O. Beatty Jr, Moving bed heat transfer: I. Effect of interstitial gas with fine particles, *Chem. Engng Prog. Symp. Ser.* **59,** 122–128 (1963).
30. J. K. Spelt, C. E. Brennen and R. H. Sabersky, Heat transfer to flowing granular material, *Int. J. Heat Mass Transfer* **25,** 791–796 (1982).
31. M. Colakyan and O. Levenspiel, Heat transfer between moving bed of solids and immersed cylinders, *A.I.Ch.E. Symp. Ser.* **80,** 156–168 (1984).
32. V. W. Uhl and W. L. Root, III, Heat transfer to granular solids in agitated units, *Chem. Engng Prog.* **63,** 81–92 (1964).
33. T. Ohmori, M. Okazaki and R. Toei, Heat transfer coefficient in stationary heating-plane type indirect-heat agitated dryer, *J. Chem. Engng Japan* **19,** 167–172 (1986).
34. K. Malhotra and A. S. Mujumdar, Immersed surface heat transfer in a vibrated fluidized bed, *Ind. Engng Chem. Res.* **26,** 1983–1992 (1987).
35. K. Malhotra and A. S. Mujumdar, Wall-to-bed contact heat transfer rates in mechanically stirred granular beds, *Int. J. Heat Mass Transfer* **34,** 427–435 (1991).
36. J. D. Gabor, Wall-to-bed heat transfer in fluidized and packed beds, *Chem. Engng Prog. Symp. Ser.* **66,** 76–86 (1970).
37. J. Kubie and J. Broughton, A model of heat transfer in gas fluidized beds, *Int. J. Heat Mass Transfer* **18,** 289–299 (1975).
38. D. Gloski, L. Glicksman and N. Decker, Thermal resistance at a surface in contact with fluidized bed particles, *Int. J. Heat Mass Transfer* **27,** 599–610 (1984).
39. E. U. Schlünder and N. Mollekopf, Vacuum contact drying of free flowing mechanically agitated particular material, *Chem. Engng Process.* **18,** 93–111 (1984).
40. L. N. Gupta, An approximate solution of the generalized Stefan's problem in a porous medium, *Int. J. Heat Mass Transfer* **17,** 313–321 (1974).
41. M. D. Mikhailov, Exact solution of temperature and moisture distributions in a porous half-space with moving evaporation front, *Int. J. Heat Mass Transfer* **18,** 797–804 (1975).
42. S. H. Cho, An exact solution of the coupled phase change problem in a porous medium, *Int. J. Heat Mass Transfer* **18,** 1139–1142 (1975).
43. R. W. Lyczkowski and Y. T. Chao, Comparison of Stefan model with two-phase model of coal drying, *Int. J. Heat Mass Transfer* **27,** 1157–1169 (1984).
44. A. Rubin and S. Schweitzer, Heat transfer in porous media with phase change, *Int. J. Heat Mass Transfer* **15,** 43–60 (1972).
45. E. M. Parmentier, Two phase natural convection adjacent to a vertical heated surface in a permeable medium, *Int. J. Heat Mass Transfer* **22,** 849–855 (1979).
46. P. Cheng and A. K. Verma, The effect of subcooled liquid on film boiling about a vertical heated surface in a porous medium, *Int. J. Heat Mass Transfer* **4,** 1151–1160 (1981).
47. G. R. Essome and J. Orozco, An analysis of film boiling of a binary mixture in a porous medium, *Int. J. Heat Mass Transfer* **34,** 757–766 (1991).
48. P. Cheng, Film condensation along an inclined surface in a porous medium, *Int. J. Heat Mass Transfer* **24,** 983–990 (1981).
49. J. P. Gorog, T. N. Adams and J. K. Brimacombe, Regenerative heat transfer in rotary kilns, *Metall. Trans.* **13B,** 153–163 (1982).
50. P. S. Ghoshdastidar, C. A. Rhodes and D. I. Orloff, Heat transfer in a rotary kiln during incineration of solid waste, Paper number 85-HT-86, presented at the National Heat Transfer Conference, Denver, CO (1985).
51. C. A. Cook, V. A. Cundy, F. S. Larsen and J. S. Lighty, A comprehensive heat transfer model for rotary desorbers, submitted to *A.I.Ch.E. Jl* (1994).
52. J. R. Ferron and D. K. Singh, Rotary kiln transport processes, *A.I.Ch.E. Jl* **37,** 747–757 (1991).
53. K. Vafai and M. Sozen, Analysis of energy and momentum transport for fluid flow through a porous bed, *J. Heat Transfer* **112,** 690–699 (1990).
54. M. Riaz, Analytical solutions for single- and two-phase models of packed-bed thermal storage systems, *J. Heat Transfer* **99,** 489–492 (1977).
55. D. Vortmeyer and R. J. Schaefer, Equivalence of one- and two-phase models for heat transfer processes in packed beds: one dimensional theory, *Chem. Engng Sci.* **29,** 485–491 (1974).
56. T. R. Goodman, The heat-balance integral and its application to problems involving a change of phase, *Trans. ASME* **80,** 335–342 (1958).
57. T. R. Goodman, Applications of integral methods to transient nonlinear heat transfer. In *Advances in Heat Transfer* (Edited by T. F. Irvine and J. P. Hartnett), Vol. 1, pp. 51–122. Academic Press, New York (1964).
58. R. Krupiczka, Analysis of thermal conductivity in granular materials, *Int. Chem. Engng* **7,** 122–144 (1967).